Application of Iron Nitride Compound as Alternative Permanent Magnet for Designing Linear Generators to Harvest Oceanic Wave Energy

Article *in* IET Electric Power Applications · March 2020

DOI: 10.1049/iet-epa.2019.0372

CITATIONS
0

READS
66

4 authors:

Selim Molla
Ahsanullah University of Science & Tech
7 PUBLICATIONS **13** CITATIONS
SEE PROFILE

Omar Farrok
Ahsanullah University of Science & Tech
53 PUBLICATIONS **197** CITATIONS
SEE PROFILE

Md Rabiul Islam
University of Wollongong
179 PUBLICATIONS **1,391** CITATIONS
SEE PROFILE

Kashem Muttaqi
University of Wollongong
270 PUBLICATIONS **4,088** CITATIONS
SEE PROFILE

IET Electric Power Applications

Research Article

IET Journals
The Institution of Engineering and Technology

Application of iron nitride compound as alternative permanent magnet for designing linear generators to harvest oceanic wave energy

ISSN 1751-8660
Received on 1st May 2019
Revised 8th March 2020
Accepted on 25th March 2020
doi: 10.1049/iet-epa.2019.0372
www.ietdl.org

Selim Molla[1] ✉, Omar Farrok[1], Md. Rabiul Islam[2], Kashem M. Muttaqi[2]

[1]Department of Electrical and Electronic Engineering, Ahsanullah University of Science and Technology, Tejgaon, Dhaka-1208, Bangladesh
[2]School of Electrical, Computer and Telecommunications Engineering, Faculty of Engineering and Information Sciences, University of Wollongong, NSW 2522, Australia
✉ *E-mail: eee.n_selim@yahoo.com*

Abstract: Most of the conventional linear generator is constructed with either Alnico (specially AlNiCo-9) or Neodymium iron boron (NdFeB) permanent magnets (PMs) for harvesting oceanic wave energy. Alnico is a composition of aluminium (Al), nickel (Ni), and cobalt (Co) added to iron, which is its major volumetric component. Alnico has a poor magnetic energy product, and NdFeB contains a rare earth element. To overcome this issue, a recently developed rare-earth free iron nitride ($Fe_{16}N_2$) compound-based PM linear generator (PMLG) is proposed in this study as an alternative solution for avoiding rare earth material while obtaining high output power. To the best of authors' knowledge, newly invented $Fe_{16}N_2$ is not proposed, analysed, and investigated in any electrical generator. In this context, $Fe_{16}N_2$ is proposed in a linear generator as PM for producing adequate magnetic flux. For analysis and testing the performance of the proposed material, a PMLG is designed. The performances are compared for using $Fe_{16}N_2$ and AlNiCo PMs in the same PMLG design for a fair comparison. It is considered that the proposed PMLG is connected to a direct drive power take-off system. Simulation results show that the proposed PMLG having $Fe_{16}N_2$ generates 55% more electrical power than that of using AlNiCo. The voltage, current, magnetic flux linkage, power, and magnetic flux density of the proposed PMLG are investigated extensively and compared with those of AlNiCo. The finite element method is applied in the ANSYS/Maxwell software environment for testing the PMLG with the conventional and the proposed PMs as well as results are presented. The proposed design is also validated with a small laboratory prototype.

1 Introduction

The generation of electricity is very significant to make the comfort of daily human lifestyle and necessary for various industries. Most of the cases, it is produced from fossil fuels, which have some drawbacks such as importation, transportation, storage, greenhouse gas emissions, and harmful to the environment [1]. Renewable energy is one of the best effective alternatives for the generation of electricity owing to the production of clean energy, resource availability, and amicable for the global environment [2]. At present, wind [3], solar [4], and sea wave energy [5] are extensively used as renewable sources. Among these, wind energy is not available all time, and solar energy is available in the daytime only. Considering the energy density, persistency, and availability, the oceanic wave is the most popular among these. Nowadays, different types of topologies are applied to convert oceanic wave energy into electricity. Considering the location, there are two types of the converter: the onshore and offshore wave energy converter (WEC). The maintenance facility of onshore WEC is easier than that of the offshore converter, but it cannot generate much output power. On the other hand, offshore WECs can produce high power. There are three power take-off systems available, such as the turbine system, hydraulic system, and linear generator [5].

A hydrodynamic system is required to convert rough oceanic wave motion into constant motion. In the turbine system, the motion of the fluid is increased. When the high-speed fluid (seawater) hits the blades of the turbine, the electricity is produced in the stator winding. The hydraulic system consists of a floating buoy, actuator, check valves, high-pressure accumulator, low-pressure accumulator, hydraulic motor, and rotary generator. The rod of the actuator is mounted with a floating buoy, which moves upward and downward with a floating buoy. As a result, fluid flows through the check valve for which the fluid velocity increases, which rotates the hydraulic motor. The rotating shaft of the motor is connected to the electrical generator. On the other hand, the working principle of the linear generator involves the movement of the translator with the floating buoy. According to structure, longer life, robustness, and mechanical interface, the direct-drive linear generator (DDLG) used as WEC is preferable than the rotational one [6].

The electricity generation system from sea wave is described in Fig. 1. It mainly consists of a buoy, a linear generator, a rectifier, an inverter, and a transformer. A buoy is always floating on the wave of seawater. There are two effective elements in the DDLG, which are the translator and stator. The translator is connected to the floating buoy by a high tensile strength rod or rope. Due to having connect with the buoy, the translator moves in the same direction. The moving direction of the translator is vertically upward and downward. When the translator moves according to previously said direction with respect to stators, emf is induced in the winding of stator abide by Faraday's law of electromagnetic induction. The amount of induced emf is directly proportional to the rate of change of flux linkage. Simply, electrical power generation is proportional to the speed of a moving translator.

It is observable that, the translator speed is not constant. It varies with the variation of oceanic wave parameters. Therefore, the frequency of generated voltage by the electrical generator is not constant at all. But the frequency should be constant for the load. For this reason, a rectifier is needed to convert dc voltage from the produced ac voltage. Finally, the inverter supplies electric power to the load through a transformer by ensuring the required control. A longitudinal flux synchronous permanent magnet (PM) DDLG is developed in [7], where a buoy is applied to drive the piston. A novel methodology of electricity generation from the linear generator used for harvesting wave energy is introduced in [8] where despite zero vertical velocity of the translator at the end

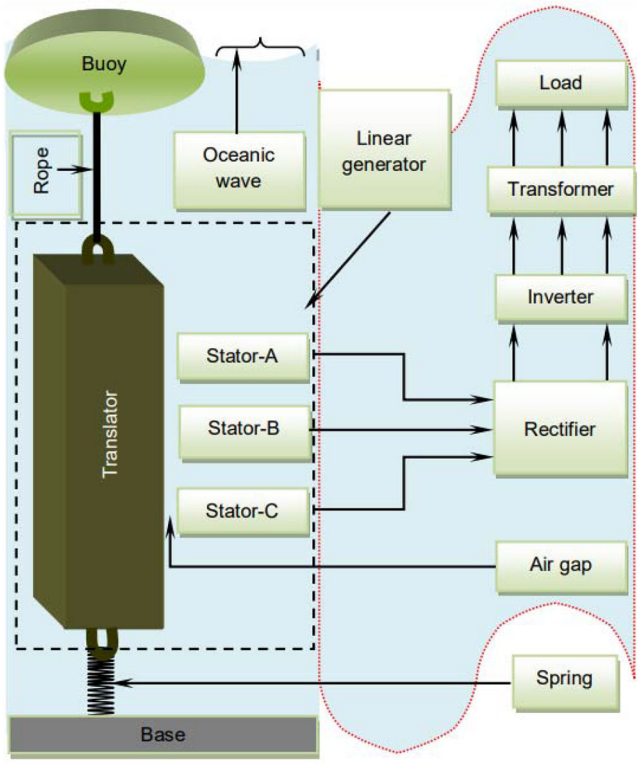

Fig. 1 *Electricity generation system from wave energy*

stops, it produces adequate electrical power. This is obtained by incorporating a driven-generator with the driver-generator through a special arrangement. An application of high-frequency transformer (HFT) is proposed in [9], which is connected to a linear generator with a variable frequency drive. For the galvanic isolation, each of the linear generators is similarly connected to an individual HFT in a wave farm.

Cogging force is another challenge of DDLG, which can be minimised by a few techniques, as mentioned in [10], such as changing the position of copper, PM, and steel. A linear generator is proposed in [11], which has low detent force and good performance even at slow speed. A methodology including analysis, design, and optimisation are presented in [12] for brushless and ironless machines. Superconducting PM linear generators are described in [13] that explain various advantages of using superconducting winding for high output power. An LG is validated both in experimentally and numerically in [14], where detent force is minimised. Lower power density and large volume are common problems for WEC. A tubular-shaped DDLG is designed in [15] to achieve high power density, whereas the flat type NdFeB PM-based DDLG is analysed and simulated in [16] where the translator weight is minimised by a split translator with secondary/supporting stator.

A real-time hybrid mathematical model is described for a wave energy converter in order to calculate the parameters easily [17]. The numerical simulation procedure is introduced for a cycloidal type wave energy converter to estimate the annual power absorption [18]. The hydrodynamic equation and power conversion equation have been formulated for oscillating water column wave energy converter where backward bent duct buoy is considered [19, 20]. A high-temperature superconductor is used to prepare the armature winding of a linear generator in which an appropriate magnetic core is proposed [21]. Considering dual wave farm, a wave energy converter is designed, in which the optimum performance is found when the WEC geometry is adapted dynamically to the sea state [22]. A smart controller is presented in [23], which maximises the absorption of wave energy. For directional incident waves, the shape of the wave energy converter has been optimised using the systematic methodology and effective computing [24].

Two types of cores are mostly used in LGs: iron core and air core, where the air-cored LGs [10] are easier for assembling. Iron cored LGs are smaller in size than that of the air-cored LGs for the same rating [17]. Most of the electrical machines are designed with conventional iron core [13, 25], which has a low magnetic saturation point. M235-35A iron core [8] and ferrite [11] are special magnetic cores. Conventional PMs are used in the existing LGs, which are discussed in [9, 10]. Among these, neodymium iron boron (NdFeB) PMs [6, 11, 12, 14] and some high graded NdFeB such as VACODYM 655HR [8], N50M [13] are mostly used in various types of LGs.

There are various research papers that present the design of PM-based rotational and linear generators. A literature review shows that most of the generators are constructed with AlNiCo-9. Recently, NdFeB PMs are proposed in several papers, which have a high magnetic energy product. However, NdFeB contains a rare earth element. On the other hand, AlNiCo-9 is a rare-earth free element, but it has poor magnetic energy product. For this reason, an alternative material iron nitride ($Fe_{16}N_2$) [26] is proposed in this paper, which can solve this dilemma. $Fe_{16}N_2$ has a high magnetic energy product and does not contain a rare earth element. Moreover, iron and nitrogen are abundant in nature. That is why; $Fe_{16}N_2$ seems to be more suitable as an alternative material in a linear generator rather than using conventional PMs.

In this paper, a DDLG is proposed where a newly reported iron nitride compound, $Fe_{16}N_2$, is used as PMs to create a magnetic field. Simulation results exhibit excellent features of the proposed $Fe_{16}N_2$-based DDLG compared to the existing one, which is further validated by experimental results.

2 Properties of PM

PM is an active material for the construction of a linear generator. Historical development and properties of PMs with maximum energy products (MEPs) are described in the following sections.

2.1 Development history of PM

In 1916, KS steel-based PM is introduced [27]. The MEP of this material is below 20 kJ/m^3. In 1930, another PM named MK steel is launched, which has a larger MEP than that of KS steel-based PM. AlNiCo-9 is a PM with high MEP (80 kJ/m^3), which has been produced since 1960. Ferrite is another type of PM that has lower MEP in comparison to AlNiCo-9, although these are produced nearly the same time. Compared to AlNiCo-9, samarium cobalt (SmCo) is a more powerful magnet manufactured in around 1969 with MEP of 160 kJ/m^3, which was further increased to around 240 kJ/m^3. NdFeB PM has a large MEP than any other PMs. Only NdFeB and SmCo among all PMs contain rare earth materials. AlNiCo-9 is the most powerful PM among all rare-earth free PMs. The global production of NdFeB PM was increased rapidly from 1990. However, it falls from 2007 because of the unavailability of materials [28].

2.2 Effect of temperature in PM

The temperature effect is very significant in the performance of any PM linear generator (PMLG) [29]. Due to demagnetisation of PM, the LG cannot produce much output power. In general, the temperature rise is one of the major causes of demagnetisation. The characteristic curves of N28EH PM at different temperatures are illustrated in Fig. 2. N28EH is a family member of neodymium iron boron PM.

Characteristics of N28EH show that the remanence flux density (B_{rem}) is 0.99 T while the machine is operated at 100°C. The coercive field strength and knee point at that temperature are −1340 kA/m and 0.86 T, respectively. At 60°C, the coercivity, knee point, and B_{rem} of this material are −1750 kA/m, 0.95 T, and 1.05 T, respectively (Fig. 2). From the analysis, it is found that DDLG made of N28EH generates much output power up to 60°C. But it cannot produce enough electrical power higher than 60°C.

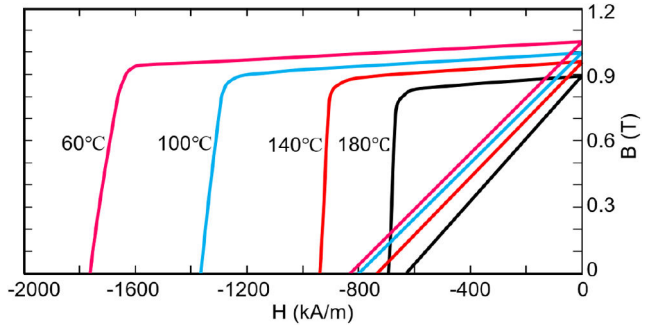

Fig. 2 *Characteristics of N28EH NdFeB PM at different temperatures*

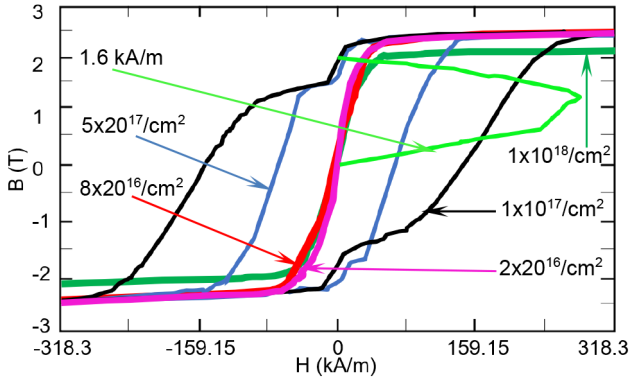

Fig. 3 *Hysteresis loops and energy product of $Fe_{16}N_2$ PM*

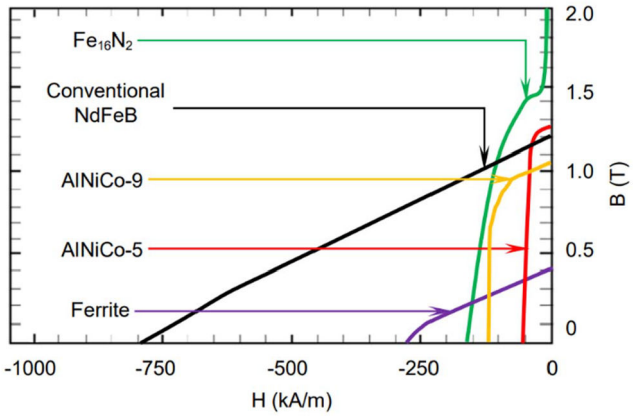

Fig. 4 *Comparison among different types of PM*

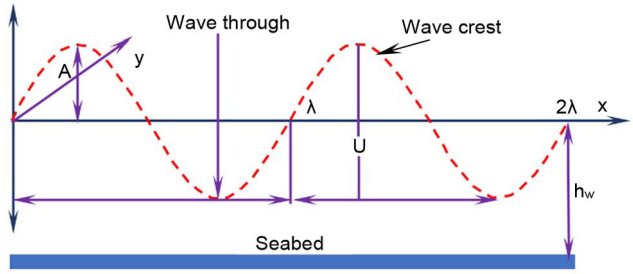

Fig. 5 *Model of sea wave*

2.3 Iron nitride PM

This type of PM is the compound of rare-earth free material: iron and nitride. Iron nitride compound has high coercivity, large remanence, and energy product. The hysteresis loops [26] and energy products of this PM are plotted in Fig. 3. The magnetic properties of $Fe_{16}N_2$ are studied in order to justify its feasibility, whether it is a suitable alternative PM instead of SmCo and NdFeB or not.

2.4 Comparisons among different types of PMs

The demagnetising curves of four types of PMs are shown in Fig. 4, where ferrite core exhibits very poor magnetic properties among these. For this reason, it is not suitable to be used in the generator. On the other hand, AlNiCo-5 and AlNiCo-9 are popular PMs owing to their good magnetic properties, availability, and low cost. A synthesised $Fe_{16}N_2$ is the compound of iron and nitrogen. These two elements are quite available, which makes it possible for a large amount of production.

In the case of the stationary condition of the translator or no-load condition, remanence magnetism is not affected. When the reverse magnetic field is applied to a PM (due to armature current), remanence magnetism of this PM becomes low. Even due to apply the same magnetic field, remanence magnetism is not obtained to the original initial value. If the slope of this loop is denoted by a straight-line AB, smaller magnitude of the applied reverse field, remanence magnetism will not decrease much. On the contrary, for larger magnitude, remanence magnetism reduces much which cannot reach to the previous loop. Rather, it would follow a new loop with even lower magnitude and slope compared to AB with respect to magnetic field intensity. This phenomenon occurs in all PM-based linear generators because of the vertical movement of the translator to stators and the armature current as well.

It is shown in Fig. 4 that remanence magnetism of $Fe_{16}N_2$ is the highest among all PMs, whereas the coercive force of this material is also higher than AlNiCo-5 and AlNiCo-9. Therefore, for its availability and good features, it is selected to be applied in the proposed DDLG design.

3 Mathematical model

Generally, the sea wave is considered as a linear wave. The mathematical model of oceanic wave and DDLG is described in the following section.

3.1 Generalised model for sea wave

The generalised wave of the ocean is depicted in Fig. 5 in which the xy plane is the surface of the sea, λ denotes the wavelength, and h_w is the depth of water [30, 31]. In the x-direction, the components of y are considered zero as the propagates of the wave, $z = -h_w$ is the seabed, and the sea surface is considered coincides in which $z = 0$. In general, this wave is explained as

$$\xi = M\cos(kx - \omega t) \tag{1}$$

$$\omega = \sqrt{gk\tan(kh_w)} \tag{2}$$

where k is the wavenumber ($k = 2\pi/\lambda$), ω is the frequency, and the waveform's amplitude is D. The water wave is related to the frequency and wavenumber. Alternatively, it is considered the relation between the velocity of wave or phase speed, S, the wavelength, λ, and g the gravitational constant. The velocity of the wave, along with the x-direction, is expressed as follows:

$$S = \sqrt{\frac{g\lambda}{2\pi}\tan\left(\frac{2\pi}{\lambda}h_w\right)} \tag{3}$$

From (1) and (3), the wave velocity along with the x-direction only, but it also has the velocity along with the z-direction. Hence, oceanic wave's velocity is a vector which depends on x, y, z, and t, where t denotes the time. In order to get a complete expression of sea waves, x, y, and z components are required to calculate. The motion of the sea wave can be described as follows:

$$S(x, y, z, t) = \{X(x, y, z, t),\ Y(x, y, z, t),\ Z(x, y, z, t)\}$$

where $S(x, y, z, t)$ denotes the velocity of sea wave and $X(x, y, z, t)$, $Y(x, y, z, t)$, and $Z(x, y, z, t)$ are the components along with the x, y, and z, respectively. The components of y are considered zero in case of sea wave and the components of x and z can be described as follows:

$$X = M\omega \frac{\cos\{k(z+h_w)\}}{\sin(kh_w)}\cos(kx-\omega t) \tag{4}$$

$$Z = M\omega \frac{\sin\{k(z+h_w)\}}{\sin(kh_w)}\sin(kx-\omega t) \tag{5}$$

3.2 Shallow water wave model

The mathematical model of oceanic wave considering shallow water is illustrated as

$$X = A\omega \frac{\cosh\{k(z+P_{\mathrm{w}})\}}{\sinh(kP_{\mathrm{w}})}\cos(kx-\omega t) \tag{6}$$

$$Z = A\omega \frac{\sinh\{k(z+p_{\mathrm{w}})\}}{\sinh(kP_{\mathrm{w}})}\sin(kx-\omega t) \tag{7}$$

$$\frac{e^{k(z+P_{\mathrm{w}})}+e^{-k(z+P_{\mathrm{w}})}}{e^{kP_{\mathrm{w}}}-e^{-kP_{\mathrm{w}}}} \cong \frac{e^{k(z+P_{\mathrm{w}})}}{e^{kP_{\mathrm{w}}}} = e^{kP_{\mathrm{w}}} \tag{8}$$

$$\frac{e^{k(z+P_{\mathrm{w}})}-e^{-k(z+P_{\mathrm{w}})}}{e^{kP_{\mathrm{w}}}-e^{-kP_{\mathrm{w}}}} \cong \frac{e^{k(z+P_{\mathrm{w}})}}{e^{kP_{\mathrm{w}}}} = e^{kP_{\mathrm{w}}} \tag{9}$$

$$\tanh(kP_{\mathrm{w}}) = \frac{e^{kP_{\mathrm{w}}}-e^{-kP_{\mathrm{w}}}}{e^{kP_{\mathrm{w}}}+e^{-kP_{\mathrm{w}}}} \cong \frac{e^{kP_{\mathrm{w}}}}{e^{kP_{\mathrm{w}}}} = 1 \tag{10}$$

where P_{w} denotes the water depth, A and U are the amplitude and height of sea wave, respectively, g is the gravitational acceleration (9.81 m/s^2), v describes the phase speed, ω is the angular velocity, and z is the vertical distance. Hence, (6) and (7) can be described as follows:

$$X_{\mathrm{D}} \cong A\omega e^{kP_{\mathrm{w}}}\cos(kx-\omega t) \tag{11}$$

$$Z_{\mathrm{D}} \cong A\omega e^{kP_{\mathrm{w}}}\sin(kx-\omega t) \tag{12}$$

If kP_{w} is greater than 1,

$$\omega = \sqrt{gk\tan h(kP_{\mathrm{w}})} \tag{13}$$

and the phase speed can be mentioned as follows:

$$v = \sqrt{\frac{g}{2}} \tag{14}$$

3.3 Output voltage, current, and power of proposed DDLG

Due to the existence of a magnetic field around the stator, the movement of the translator generates a voltage. The terminal voltage of the stator can be expressed by

$$V_\phi = E_A + E_d + E_q \tag{15}$$

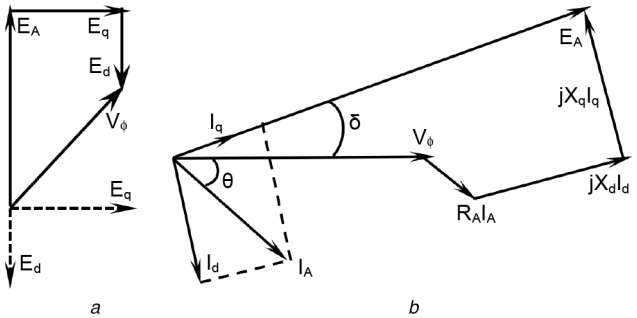

Fig. 6 *Phasor diagram of the linear generator*
(a) Phase voltage, ***(b)*** Generated and terminal voltages

where E_A is the internal produced voltage, E_d denotes the direct axis (d-axis) voltage, and E_q is the quadrature axis voltage, as shown in Fig. 6*a*. The voltage caused by armature reaction in case of each component can be expressed by

$$E_d = -jx_dI_d \tag{16}$$

$$E_q = -jx_qI_q \tag{17}$$

Therefore, (15) becomes

$$V_\phi = E_A - jx_dI_d - jx_qI_q \tag{18}$$

Now, the armature resistance and self-reactance must be involved. If armature's self-reactance, X_a is independent of rotor angle, it is added simply to the direct and quadrature reactances of armature reaction to represent the direct and quadrature synchronous reactances, respectively, of the generator as

$$X_d = x_d + X_A \tag{19}$$

$$X_q = x_q + X_A \tag{20}$$

The voltage drop across the resistance of armature is equal to the product of armature current and armature resistance. Hence, (18) becomes

$$V_\phi = E_A - jx_dI_d - jx_qI_q - R_AI_A \tag{21}$$

The vector diagram is shown in Fig. 6*b* in which both I_d and I_q relates to the output power. The flowing current through the armature resistance is resolved into two components. The phase angle between I_A and E_A is $\theta+\delta$, where θ is the angle of power factor and δ is the power angle. Normally, the power-factor angel is known earlier, not the load angle. The produced output power of DDLG can be written as follows:

$$P = \frac{3E_AV_\phi\sin\delta}{X_{\mathrm{s}}} \tag{22}$$

$$P = 3V_\phi I_d\cos(90^\circ-\delta) + 3V_\phi I_q\cos\delta \tag{23}$$

$$\begin{aligned} P &= P_d + P_q \\ &= 3V_\phi I_d\cos(90^\circ-\delta) + 3V_\phi I_q\cos\delta \\ &= 3V_\phi I_d\sin\delta + 3V_\phi I_q\cos\delta \end{aligned} \tag{24}$$

The current of the direct axis is expressed as

$$I_d = \frac{E_A - V_\phi\cos\delta}{X_d} \tag{25}$$

and the current of the quadrature axis is expressed as

$$I_q = \frac{V_\phi\sin\delta}{X_q} \tag{26}$$

Now putting the magnitude of direct axis and quadrature axis currents in (24) yields

$$\begin{aligned} P &= 3V_\phi\left(\frac{E_A - V_\phi\cos\delta}{X_d}\right)\sin\delta + 3V_\phi\left(\frac{V_\phi\sin\delta}{X_q}\right)\cos\delta \\ &= \frac{3V_\phi E_A}{X_d}\sin\delta + 3V_\phi^2\left(\frac{1}{X_q}-\frac{1}{X_d}\right)\sin\delta\cos\delta \end{aligned}$$

Since $\sin\delta\cos\delta = 1/2\sin 2\delta$, this expression minimises to

$$P = \frac{3V_\phi E_A}{X_d}\sin\delta + \frac{3V_\phi^2}{2}\left(\frac{X_d - X_q}{X_dX_q}\right)\sin 2\delta \tag{27}$$

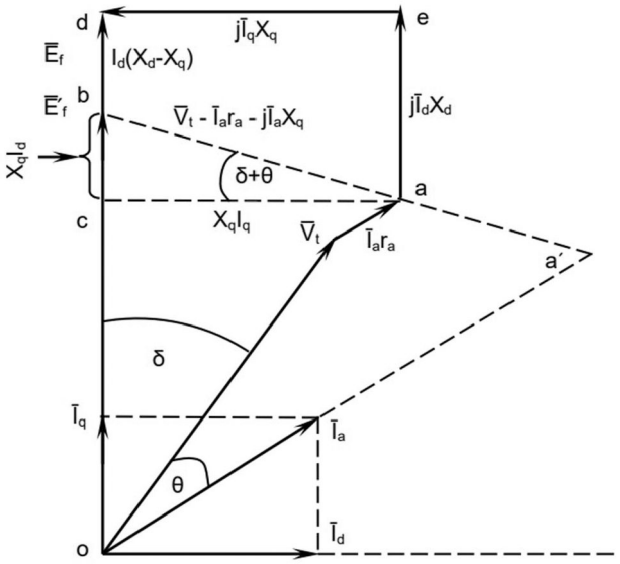

Fig. 7 *Phasor diagram of the DDLG*

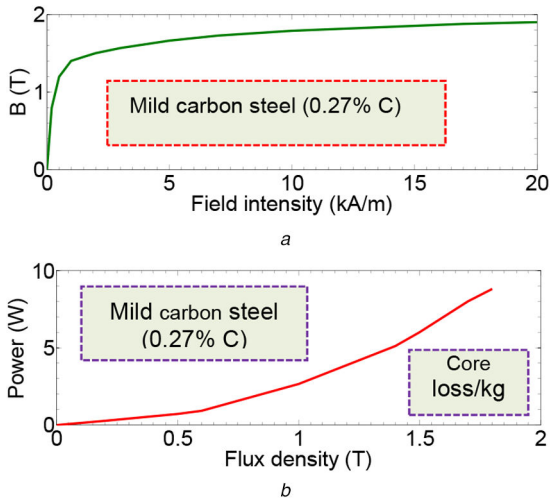

Fig. 8 *Magnetic properties of the core*
(a) Magnetising curve, *(b)* Core loss curve

The relationship between voltage and current is applicable in both transient and steady-state analysis of the proposed DDLG. Phasor diagram of generated output voltage and load current of the DDLG are drawn in Fig. 7, where *ob* is represented by E'_f, which can be expressed as

$$\bar{E}'_f = V_t + \bar{I}_a r_a + j\bar{I}_a X_q \tag{28}$$

where r_a and I_a are the winding resistance and current of the armature, respectively; V_t is the terminal voltage, E'_f represents the exciting voltage, and X_q denotes the reactance in the q-axis. The voltage equation of the DDLG can be written as

$$\bar{E}_f = V_t + \bar{I}_a r_a + j\bar{I}_a X_q + j\bar{I}_d(X_d - X_q) \tag{29}$$

where X_d and I_d represent the reactance and current in the d-axis, respectively. In the DDLG, V_t is behind of E'_f. Therefore, the voltage V_t is found as

$$\bar{V}_t = \bar{E}f + J(X_d - X_q)\bar{I}_d + J\bar{I}_a X_q + \bar{I}_a r_a \tag{30}$$

4 Design of the proposed DDLG

The DDLG is mainly constructed with three active materials, such as mild carbon steel core, copper wire, and $Fe_{16}N_2$ PM. The proposed core contains 0.27% carbon. The magnetising characteristics and core loss curves of this core are plotted in Fig. 8.

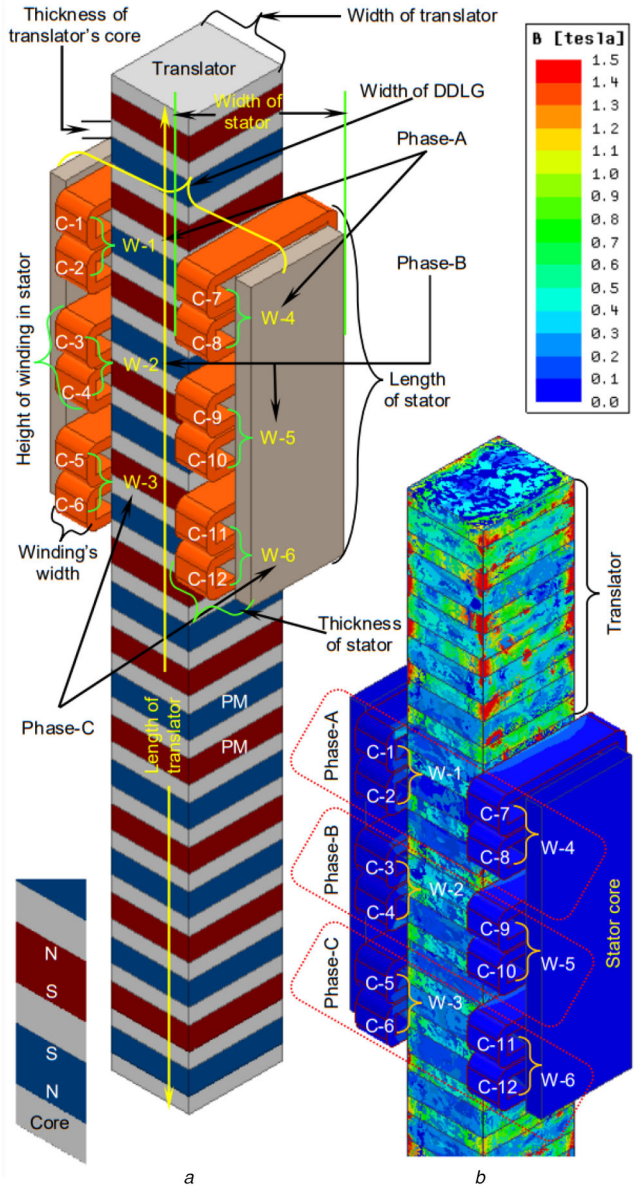

Fig. 9 *The proposed DDLG*
(a) Basic structure, ***(b)*** Its magnetic flux distribution

The magnetic flux density of the core is 1.9 T at 20 kA field intensity, and the core loss is 8.8 W/kg at 1.8 T. This core has some advantages, such as its availability, low cost, and high tensile strength.

The basic structure of the proposed linear generator is presented in Fig. 9*a*. It mainly consists of a translator and three sets of stators, namely Phase-A, Phase-B, and Phase-C. The translator is made of the magnetic core and $Fe_{16}N_2$ PM, where *N* and *S* stand for the North and the South poles of $Fe_{16}N_2$-based PM, respectively. The air gap between the translator and the stator is 3 mm. On the other hand, stators are made of copper windings and mild carbon steel cores. In Fig. 9*a*, *C*-1, *C*-2,…, *C*-12 are the short form of copper coils. Each winding denoted by *W*-1, *W*-2,…, *W*-6 consists of two coils. The translator is connected to a floating buoy by a high tensile strength rope or rod.

As the buoy moves vertically with the oceanic wave, the translator also moves along with the buoy to stationary stators. The dimensions of the proposed linear generator are presented in Table 1.

The magnetic flux density of the proposed DDLG is shown in Fig. 9*b*. The magnetic flux is properly distributed in the magnetic cores of the DDLG. Maximum flux is obtained at the red colour, and minimum flux is found in blue colour.

Table 1 Dimension of the proposed DDLG

Name of the parameters	Value
width of DDLG, m	0.506
translator's width, m	0.2
winding's width, m	0.081
width of magnetic core in stator, m	0.11
load resistance, Ω	4
height of stator's winding, m	0.094
height of core (thickness) in translator, m	0.04

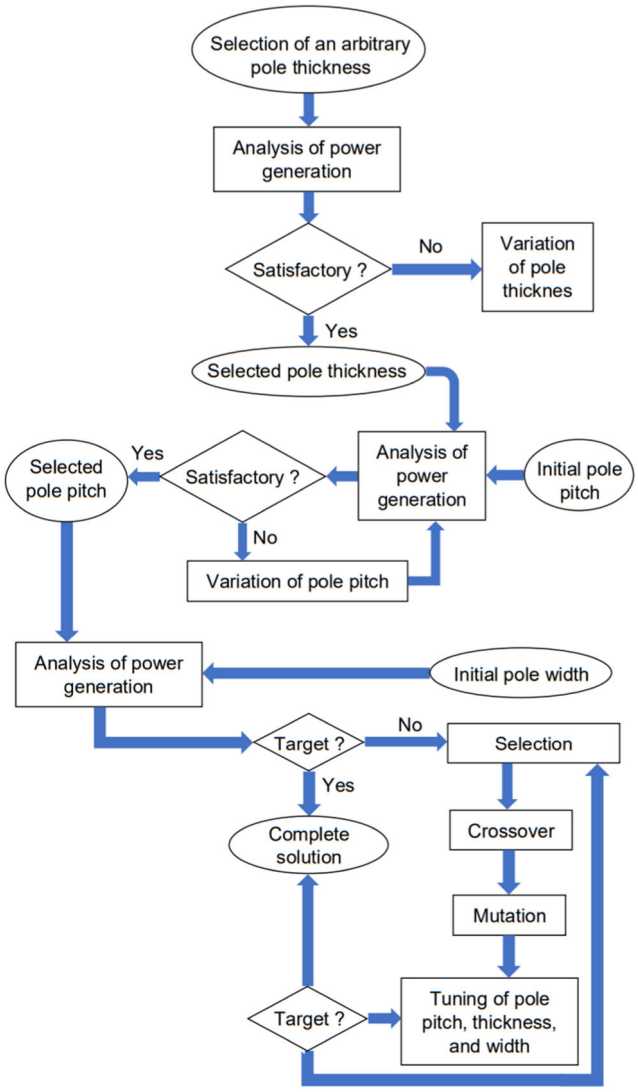

Fig. 10 *Design optimisation method of the proposed DDLG*

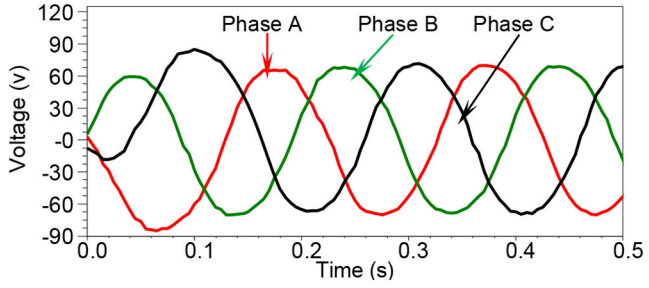

Fig. 11 *Generated voltage of the proposed DDLG*

The optimisation is carried out with varying key parameters of the linear generator, as shown in Fig. 10. The thickness and width of the magnetic pole shoe are taken into consideration along with pole pitch. During the optimisation process, the volume of the proposed DDLG is minimised for producing the rated output power. The optimised DDLG is compact enough and generates rated power at the desired voltage.

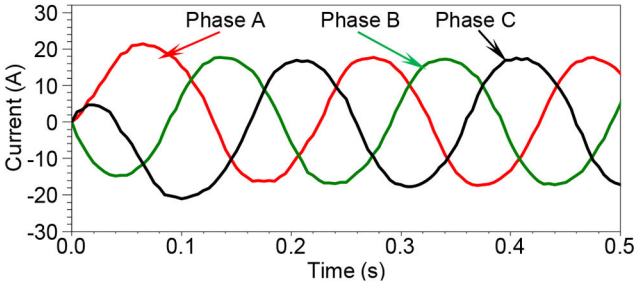

Fig. 12 *Load current of the proposed DDLG*

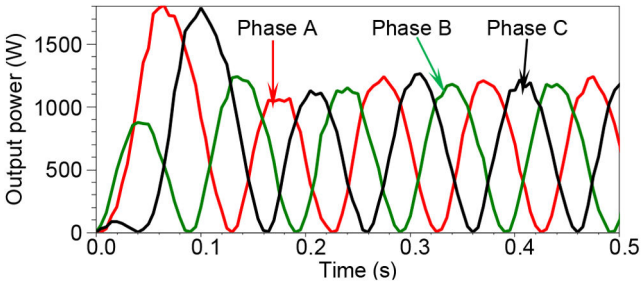

Fig. 13 *Output power of the proposed DDLG*

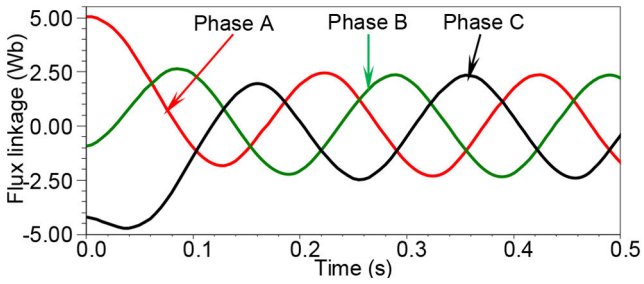

Fig. 14 *Flux linkage of the proposed DDLG*

5 Results and discussion

The vertically moving speed of the translator is considered 1 m/s. Generated voltages (for each phase) of the proposed DDLG are presented in Fig. 11. The rms value of the voltage of Phase-A, Phase-B, and Phase-C is 49.07, 48, and 50.25 V, respectively. This machine generates a peak voltage of 60.395, 67.882, and 71.06 V in Phase-A, Phase-B, and Phase-C, respectively. Load currents of the DDLG (for each phase) are plotted in Fig. 12 where the rms magnitudes are 12.45, 12.14, and 12.32 A for Phase-A, Phase-B, and Phase-C, respectively. This generator delivers the peak current of 17.76, 17.17, and 17.42 A for Phase-A, Phase-B, and Phase-C, respectively. The instantaneous output powers at different phases are plotted in Fig. 13.

In Fig. 14, 1.73, 1.66, and 1.65 Wb are obtained from Phase-A, Phase-B, and Phase-C, respectively. The smooth flux linkage indicates that the core can conduct proper magnetic flux. The power loss curve of the proposed DDLG is plotted in Fig. 15, where eddy current loss and core loss have been focused. The comparison between the terminal voltages of $Fe_{16}N_2$ and AlNiCo-9-based DDLG is shown in Fig. 16.

The proposed generator produces a much higher voltage than the other generator. From Fig. 17, it is seen that the load currents of $Fe_{16}N_2$-based DDLG is higher than that of AlNiCo-9-based DDLG.

The rms power comparison of AlNiCo-9- and $Fe_{16}N_2$-based DDLG is presented in Fig. 18. The proposed generator made of $Fe_{16}N_2$ generates higher rms output power between them. The average output rms power of this machine is 1273.43 W.

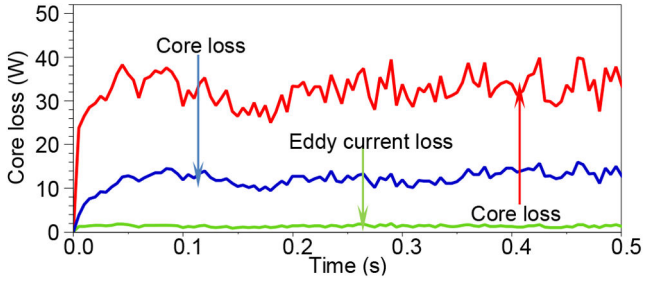

Fig. 15 *Core loss curve of the proposed DDLG*

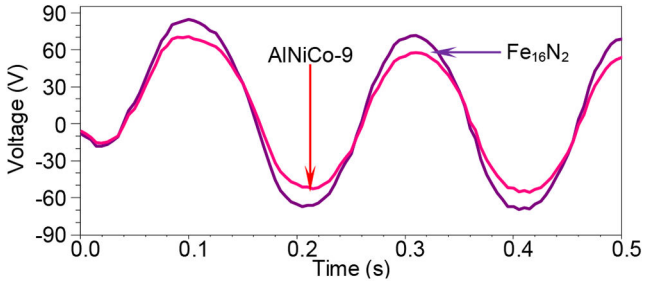

Fig. 16 *Comparison of terminal voltages between AlNiCo-9- and $Fe_{16}N_2$-based DDLGs*

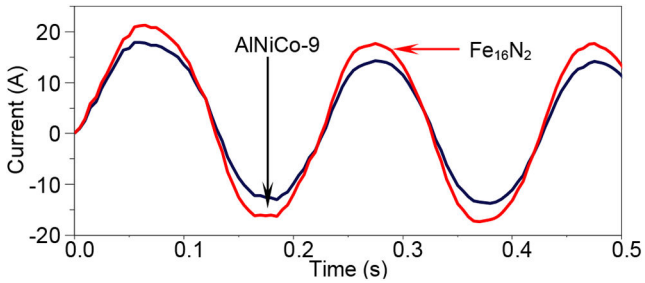

Fig. 17 *Comparison of load currents between AlNiCo-9- and $Fe_{16}N_2$-based DDLGs*

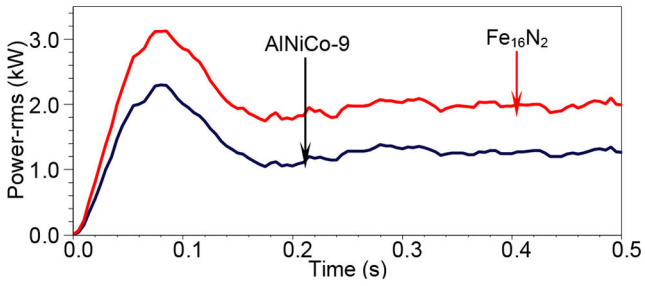

Fig. 18 *Comparison of rms power between AlNiCo-9- and $Fe_{16}N_2$-based DDLG*

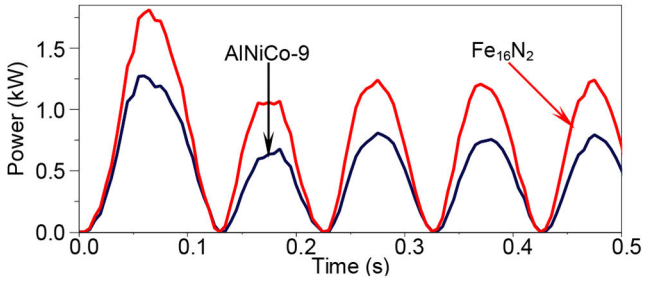

Fig. 19 *Comparison of output power between AlNiCo-9-based DDLG and $Fe_{16}N_2$-based DDLG*

The output powers for $Fe_{16}N_2$- and AlNiCo-9-based linear generators are compared in Fig. 19, where the output power of the proposed generator is much higher than that of the other. The

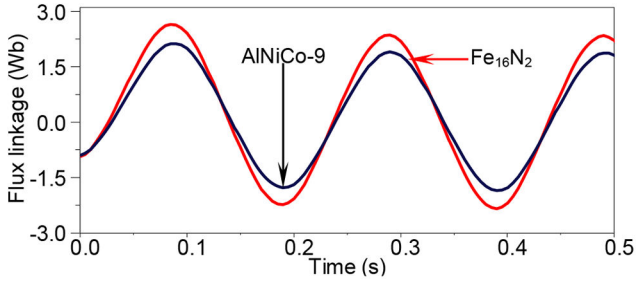

Fig. 20 *Comparison of flux linkage between AlNiCo-9 and $Fe_{16}N_2$ based DDLGs*

Table 2 Comparison between AlNiCo-9- and $Fe_{16}N_2$-based linear generator

Name of the parameters	AlNiCo-9	$Fe_{16}N_2$
peak generated voltage, V	57.48	71.06
peak load current, A	−14.37	−17.76
peak flux linkage, Wb	1.51	1.78
peak instantaneous power, W	826.2	1262.6
average output rms power, W	1273.43	1974.8

comparison between flux linkages of iron nitride and Alnico-9-based DDLG is shown in Fig. 20.

Iron nitride PM-based DDLG has higher flux linkage than that of the other. The comparative results for different parameters of the DDLG using AlNiCo-9 and $Fe_{16}N_2$ at the time, $t = 310$ ms are presented in Table 2.

It is found that the PMLG with proposed $Fe_{16}N_2$ can produce much higher voltage, current, and power than that of using AlNiCo-9. The Mesh plot of the proposed linear generator is shown in Fig. 21. Mesh setup is one of the key elements to analyse the linear generator. It is also very essential for finite elements analysis system.

In general, the triangular mesh is considered for 2D, whereas tetrahedral shape is applied in case of 3D analysis. Since the proposed machine is analysed in 3D, therefore, the tetrahedral shape is selected before carrying out the simulation. For this work, fine mesh setup is considered, so that simulation results become accurate. Only PM and magnetic cores are included in mesh setup for a translator.

On the other hand, the stator core and copper winding are considered during the mesh setup of the stator. For this reason, stator mesh looks disorderly and dense than that of the translator because of the bend of wire in the winding. To test the performance of the proposed design, a downscale prototype (8:1) using AlNiCo-9 is constructed, as shown in Fig. 22. Fig. 23 shows a photograph of the experimental setup for different magnetic materials characterisation.

The stroke length of the generator is 0.356 m, the time period is 1.4 s, and power rating is 200 W. Peak value of the terminal voltage at no-load condition is 38 V (simulation), whereas the same for the prototype is 37 V, approximately. The comparisons are illustrated in Fig. 24 where the voltage wave shapes are similar to each other, and both are producing 50 Hz voltage.

The proposed generator produces electrical power under the condition of applying mechanical force to the translator. As the translator consists of translator core and PM one after another, cogging force components, Force_x, Force_y, and Force_z vary during operation, which is shown in Fig. 25.

6 Conclusion

The problem with NdFeB is that it is not a rare earth free magnet which means it has a limited stock in the whole world. The generation of large scale electrical power from the oceanic wave would require a bulk amount of PMs. On the contrary, the existing rare-earth free magnets such as ferrites, AlNiCo-5, and AlNiCo-9 have low remanence magnetism and coercive force, as illustrated in Fig. 4. In these circumstances, a suitable replacement of NdFeB

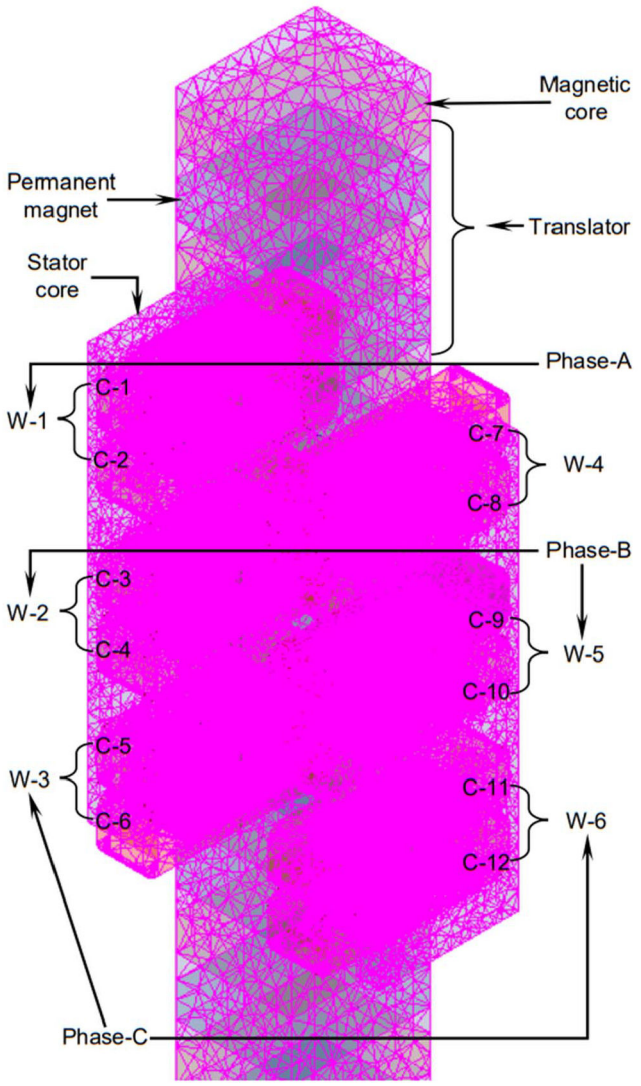

Fig. 21 *Mesh plot of the proposed DDLG*

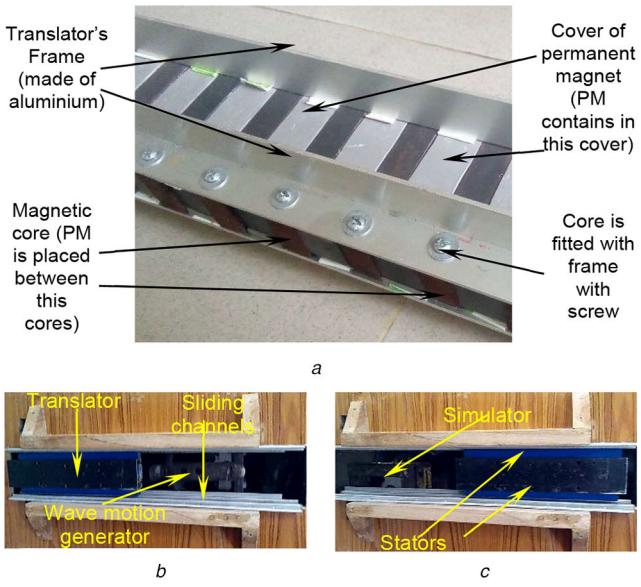

Fig. 22 *Simulator and prototype of the DDLG with AlNiCo-9*
(a) Translator, ***(b)*** Position of a translator at the left, ***(c)*** Right-hand side

is required for the persistent, sustainable development of PMLGs. The proposed design concept is the outcome from the concern of finding the best alternative of rare earth magnets, as all the existing rear earth free PMs have poor magnetic energy product. Ferrites and AlNiCo-5 are not considered to be used in the DDLG because

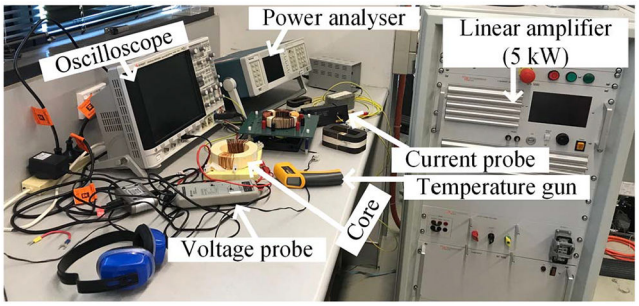

Fig. 23 *Experimental setup to characterise magnetic materials*

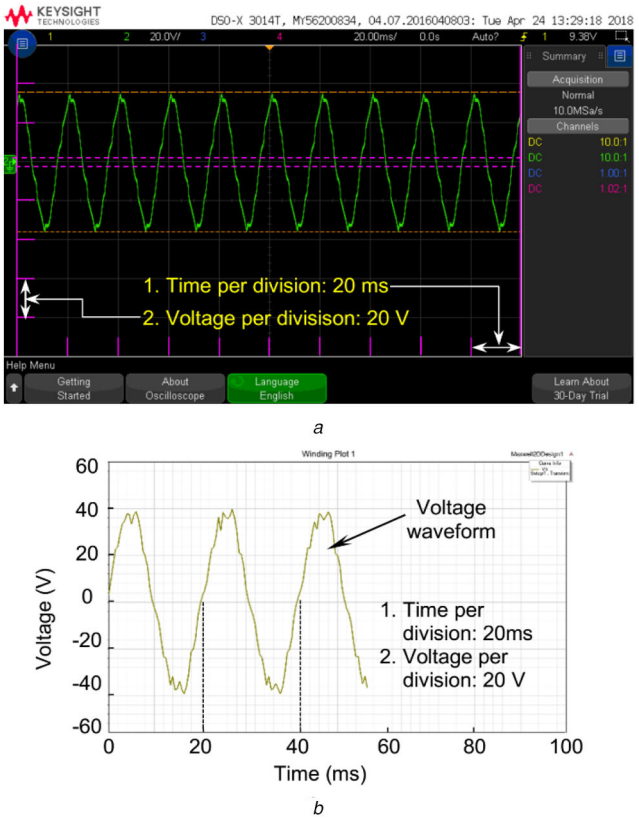

Fig. 24 *Comparison of voltages*
(a) Experimental, ***(b)*** Simulation

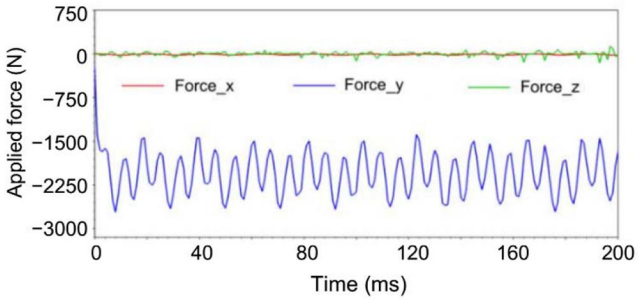

Fig. 25 *Applied force to the translator*

of their poor magnetic properties. Simulation results show that using the proposed $Fe_{16}N_2$ in the DDLG as PMs, 17.9% more magnetic flux linkage, 23.6% more peak voltage, and hence much higher electrical power can be obtained than that of using the AlNiCo-9. For this reason, $Fe_{16}N_2$ is proposed as the best alternative PMs for designing linear machines to be used as a wave energy converter. To test the performance of the proposed DDLG and accuracy of the simulation results, a prototype is constructed using AlNiCo-9 as $Fe_{16}N_2$ is not available in the market. Generated voltages are compared for both the experimental and simulated

results for using the same DDLG and other materials to make a fair comparison.

7 References

[1] Bose, B.K.: 'Global warming: energy, environmental pollution, and the impact of power electronics', *IEEE Ind. Electron. Mag.*, 2010, **4**, (1), pp. 6–17

[2] Panwar, N.L., Kaushik, S.C., Kotharia, S.: 'Role of renewable energy sources in environmental protection: a review', *Renew. Sustain. Energy Rev.*, 2011, **15**, (3), pp. 1513–1524

[3] Lin, M., Hao, L., Li, X.*, et al.*: 'A novel axial field flux-switching permanent magnet wind power generator', *IEEE Trans. Magn.*, 2011, **47**, (10), pp. 4457–4460

[4] Xie, W.T., Dai, Y.J., Wang, R.Z.*, et al.*: 'Concentrated solar energy applications using fresnel lenses: a review', *Renew. Sustain. Energy Rev.*, 2011, **15**, (6), pp. 2588–2606

[5] Drew, B., Plummer, A.R., Sahinkaya, M.N.: 'A review of wave energy converter technology', *Proc. Inst. Mech. Eng. A, J. Power Energy*, 2009, **223**, (8), pp. 887–902

[6] Memon, A.H., Ibrahim, T.B., Perumal, N.: 'Portable and pico-scale linear generator for wave energy conversion'. Int. Conf. Intell. Advanced System, Kuala Lumpur, Malaysia, June 2014, pp. 1–4

[7] Zheng, P., Chen, A., Thelin, P.*, et al.*: 'Research on a tubular longitudinal flux PM linear generator used for free-piston energy converter', *IEEE Trans. Magn.*, 2007, **43**, (1), pp. 447–449

[8] Farrok, O., Islam, M.R., Muttaqi, K.M.*, et al.*: 'Design and optimization of a novel dual-port linear generator for oceanic wave energy conversion', *IEEE Trans. Ind. Electron.*, 2020, **67**, (5), pp. 3409–3418

[9] Islam, M.R., Farrok, O., Rahman, M.A.*, et al.*: 'Design and characterization of advanced magnetic material based core for isolated power converters used in wave energy generation system', *IET Electr. Power Appl.*, 2019 (accepted), doi: 10.1049/iet-epa.2019.0299

[10] Hodgins, N., Keysan, O., McDonald, A.S.*, et al.*: 'Design and testing of a linear generator for wave-energy applications', *IEEE Trans. Ind. Electron.*, 2012, **59**, (5), pp. 2094–2103

[11] Huang, L., Yu, H., Hu, M.*, et al.*: 'Research on a tubular primary permanent-magnet linear generator for wave energy conversions', *IEEE Trans. Magn.*, 2013, **49**, (5), pp. 1917–1920

[12] Stamenkovic, I., Milivojevic, N., Schofield, N.*, et al.*: 'Design, analysis, and optimization of ironless stator permanent magnet machines', *IEEE Trans. Power Electron.*, 2013, **28**, (5), pp. 2527–2538

[13] Kiran, M.R., Farrok, O., Guo, Y.: 'Superconducting linear machines for electrical power generation from the oceanic wave', in '*Advanced linear machines and drive systems*' (Springer Nature Singapore Pte Ltd., Singapore, 2018), pp. 281–302, doi: 10.1007/978-981-13-9616-8_8

[14] Farrok, O., Islam, M.R.: '*Advanced electrical machines for oceanic wave energy conversion*', *Renewable Energy and the Environment*, (Springer Nature Singapore Pte Ltd., Singapore, 2018), pp. 115–141, doi: 10.1007/978-981-10-7287-1_4

[15] Cipriani, M.G., Curto, D., Dio, V.D.*, et al.*: 'Minimization of detent force in a 1 kW linear permanent magnet generator for the conversion of sea waves energy: numerical and experimental validation'. IEEE Int. Magn. Conf., Beijing, China, 2015, pp. 1–1

[16] Farrok, O., Islam, M.R., Sheikh, M.R.I.*, et al.*: 'Design and analysis of a novel lightweight translator permanent magnet linear generator for oceanic wave energy conversion', *IEEE Trans. Magn.*, 2017, **53**, (11), Article ID: 8207304

[17] Börner, T., Alam, M.: 'Real time hybrid modeling for ocean wave energy converters', *Renew. Sustain. Energy Rev.*, 2015, **43**, pp. 784–795

[18] Siegel, S.G.: 'Numerical benchmarking study of a cycloidal wave energy converter', *Renew. Energy*, 2019, **134**, pp. 390–405

[19] Sheng, W.: 'Motion and performance of BBDB OWC wave energy converters: I, hydrodynamics', *Renew. Energy*, 2019, **138**, pp. 106–120

[20] Sheng, W.: 'Power performance of BBDB OWC wave energy converters', *Renew. Energy*, 2019, **132**, pp. 709–722

[21] Molla, S., Farrok, O., Islam, M.R.*, et al.*: 'Analysis and design of a high performance linear generator with high grade magnetic cores and high temperature superconducting coils for oceanic wave energy conversion', *IEEE Trans. Appl. Supercond.*, 2019, **29**, (2), Article ID: 5201105

[22] Bergillos, R.J., Delgado, C., Allen, J.*, et al.*: 'Wave energy converter configuration in dual wave farms', *Ocean Eng.*, 2019, **178**, pp. 204–214

[23] Li, L., Yuan, Z., Gao, Y.: 'Maximization of energy absorption for a wave energy converter using the deep machine learning', *Energy*, 2018, **165**, pp. 340–349

[24] Esmaeilzadeh, S., Alam, M.: 'Shape optimization of wave energy converters for broadband directional incident waves', *Ocean Eng.*, 2019, **174**, pp. 186–200

[25] Farrok, O., Islam, M.R., Sheikh, M.R.I.*, et al.*: 'Oceanic wave energy conversion by a novel permanent magnet linear generator capable of preventing demagnetization', *IEEE Trans. Ind. Appl.*, 2018, **54**, (6), pp. 6005–6014

[26] Jiang, Y., Mehedi, M.A., Fu, E.*, et al.*: 'Synthesis of $Fe_{16}N_2$ compound free-standing foils with 20 MGOe magnetic energy product by nitrogen ion-implantation', *Nat. Sci. Rep.*, 2016, **6**, Article ID: 25436

[27] Shaw, S., Constantinides, S.: 'Permanent magnets: the demand for rare earths'. Int. Rare Earths Conf., Hong Kong, China, May 2016

[28] Zepf, V.: 'An overview of the usefulness and strategic value of rare earth metals', in '*Rare Earths Industry*' (Elsevier, Amsterdam, The Netherlands, 2016), Chapter-1, pp. 3–17

[29] Bashir, M.S., Farrok, O., Islam, M.R.*, et al.*: 'N28EH permanent magnet based linear generator to prevent demagnetization during oceanic wave energy conversion'. Int. Conf. Elect. Mach. Syst., Jeju, South Korea, 2018, pp. 1836–1841

[30] Molla, S., Farrok, O.: 'Water cooled chiller based HVAC system used in a linear generator for oceanic wave energy conversion'. Int. Conf. Advances in Sci. Eng. Robot. Technol., Dhaka, Bangladesh, 3–5 May 2019

[31] Farrok, O., Islam, M.R., Sheikh, M.R.I.: 'Analysis of the oceanic wave dynamics for generation of electrical energy using a linear generator', *J. Energy*, 2016, Article ID: 3437027